MENU Access provided by Pennsylvania State Univ SIGN IN/REGISTER SEARCH CITA

HIDEN ANALYTICAL www.HidenAnalytical.com Mass Spectrometers for Plasma Diagnostics Click Here

AIP Applied Physics Letters SUBMIT

HOME ISSUES INFO FOR AUTHORS COLLECTIONS SIGN U

Home > Applied Physics Letters > Volume 115, Issue 9 > 10.1063/1.5116910

Full . Published Online: 26 August 2019 Accepted: August 2019

Ferroelectric domain structures and temperature-misfit strain phas diagrams of $K_{1-x}Na_xNbO_3$ thin films: A phase-field study

Appl. Phys. Lett. **115**, 092902 (2019); https://doi.org/10.1063/1.5116910

Bo Wang, Hao-Nan Chen, Jian-Jun Wang[a], *and* Long-Qing Chen[a]

View Affiliations

PDF ABSTRACT FULL TEXT FIGURES TOOLS SHARE

TOPICS
- Piezoelectric materials
- Ferroelectricity
- Thin films
- Epitaxy
- Chemical compounds and components
- Microstructural properties
- Spectral methods
- Semiconductors
- Ceramics
- Phase transitions

ABSTRACT

Potassium-sodium niobate $K_{1-x}Na_xNbO_3$ (KNN) is one of the most promising lead-free piezoelectric materials. While there have been many studies on the microstructures and properties of KNN ceramics, the phase transitions and ferroelectric domain structures of KNN thin films are not well understood. In this work, we employ three-dimensional (3D) phase-field simulations to obtain the ferroelectric domain structures of KNN ($0 \le x \le 0.5$) thin films under a range of temperatures (0 K to 1300 K) and equiaxial misfit strains (−1.5% to 1.5%), based on which we establish the misfit strain-temperature phase diagrams of $KNbO_3$ and $K_{0.5}Na_{0.5}NbO_3$ thin films. We identify a wide variety of complex domain structures with coexisting ferroelectric phases, implying enhanced dielectric and piezoelectric properties. We expect this work to provide guidance for the strain engineering of domain structures and properties of KNN thin films.

Potassium-sodium niobate (KNN) is one of the most promising lead-free piezoelectric materials as a potential replacement for $PbZr_xTi_{1-x}O_3$ (PZT) for electromechanical applications in sensing, actuating, transducing, and energy harvesting.[1,2] Although pure KNN ceramics have moderate piezoelectricity ($d_{33} \sim 80$ pC/N), they can be significantly enhanced by optimizing sintering conditions,[3] phase-boundary engineering,[4,5] domain engineering,[6] texturing,[7] etc. For example, Saito *et al.* reported excellent piezoelectric performance with

d_{33} up to 416 pC/N in textured KNN-based ceramics with Li-, Ta-, and Sb-doping.[8] Subsequent record-setting piezoelectric d_{33} values have been reported in modified and highly textured KNN-based ceramics,[7] reaching as high as 500–700 pC/N (see recent review articles[4,5]) which are comparable to commercial soft PZT (350–700 pC/N).

Piezoelectric thin films with submicrometer to nanometer thicknesses have been extensively exploited for microelectromechanical systems (MEMS) applications. Although most of the existing studies have focused on PZT thin films,[9] there have also been several studies on KNN-based thin films.[10–13] The domain structure of a thin film is sensitive to the lattice misfit strain imposed by a substrate, which has been extensively utilized to tune ferroelectric,[14] electro-optical,[15] thermoelectric properties,[16,17] etc.[18] Therefore, understanding the misfit strain effect on domain structures is critical to the development of ferroelectric thin films with desired properties.

There are several reports on the domain structures in pure KNN and KNN-based thin films.[12,13,19–24] For example, Schmidbauer *et al.* employed piezoresponse force microscopy to analyze various intriguing domain patterns, including the observation of stripelike, checkerboardlike, and herringbonelike superstructures in high-quality epitaxial KNN thin films by tuning potassium composition,[20] anisotropic misfit strains from different substrates,[12,25] and film thicknesses.[21] Fujii and Wada revealed the evolution of polarization and domain patterns under an electrical field in KNN films with a composition close to $NaNbO_3$.[24] Luo *et al.* reported the stabilization of monoclinic phases by misfit strains with complex multidomain structures in slightly doped KNN thin films.[13,26] The authors also observed a phase transition between M_C and M_A phases accompanied by a drastic change in the domain morphology at an elevated temperature, which is believed to lead to enhanced piezoelectric responses.[13]

Despite many experimental works, a theoretical study on the domain structures in KNN thin films is still lacking. Previously, we developed an 8th-order Landau-Ginzburg-Devonshire (LGD) thermodynamic potential[27] and utilized it to analyze the phase transitions and dielectric and piezoelectric properties in single-domain KNN films.[28] Here, we perform 3D phase-field modeling to gain insights into the polydomain structures in (001)-oriented epitaxial $K_{1-x}Na_xNbO_3$ thin films with various chemical compositions ($0 \le x \le 0.5$) subject to different equibiaxial misfit strains (−1.5% to 1.5%) and temperatures (0 K to 1300 K). Based on the polydomain structures, we establish the misfit strain-temperature phase diagrams of $KNbO_3$ and $K_{0.5}Na_{0.5}NbO_3$ thin films, which contain the information about the phase stability, phase coexistence, and phase transitions. In particular, we identify a rich variety of heterophase domain structures with coexisting ferroelectric phases, in which enhanced dielectric and piezoelectric responses are anticipated.

The detailed formulation for the phase-field model of ferroelectric thin films can be found in

The detailed formulation for the phase-field model of ferroelectric thin films can be found in the existing literature.[29,30] The LGD coefficients of stress-free KNN single crystals are taken from Ref. 27. The elastic stiffness is adopted from Ref. 31 (c_{11} = 230 GPa, c_{12} = 90 GPa, and c_{44} = 76 GPa) and is assumed to be independent of composition. The electrostrictive coefficients are assumed to be linearly dependent on the composition and are deduced from experimental results:[32–34] $Q_{11} = 2x \times 0.166 + (1 - 2x) \times 0.13$, $Q_{12} = 2x \times (-0.072) + (1 - 2x) \times (-0.047)$, and $Q_{44} = 2x \times 0.029 + (1 - 2x) \times 0.052$, where x ($0 \le x \le 0.5$) is the sodium composition in $K_{1-x}Na_xNbO_3$. The TDGL equation is solved numerically using the semi-implicit Fourier spectral method[35] in a spatially discretized system with $128\Delta x \times 128\Delta y \times 50\Delta z$ grid points ($\Delta x = \Delta y = \Delta z = 1$ nm). The (001)-oriented film is set to 20 nm thickness with the 20 nm buffer layer as the substrate beyond which displacements in the substrate are assumed to be zero.[36] We also assume that the film thickness simulated here is sufficiently thin for precluding misfit strain relaxation via formation of dislocations. The electrical and mechanical equilibrium equations are solved at each simulation time step under short-circuit and thin-film boundary conditions,[36] respectively. In each simulation, the system starts from a random distribution of small-magnitude polarization and then relaxes for sufficiently long simulation time to ensure a nearly equilibrium state.

We perform a series of phase-field simulations to obtain domain structures of KNN thin films at various compositions, temperatures, and misfit strains. Based on the simulated domain structures, the temperature-misfit strain phase diagrams of the two end members, i.e., $KNbO_3$ and $K_{0.5}Na_{0.5}NbO_3$, are established and illustrated in Figs. 1(a) and 1(b), respectively. Similarly, the misfit strain-composition phase diagram of $K_{1-x}Na_xNbO_3$ ($0 \le x \le 0.5$) thin films at room temperature is obtained as shown in Fig. 1(c). The representative domain structures of different phase regions in the diagrams are shown in Fig. 2. For both materials, there are mainly eight different phase regions including the cubic paraelectric phase (C), three tetragonal ferroelectric phases (T) with in-plane (T_{ip}), out-of-plane (T_{op}), or mixed ($T_{a/c}$) polarization, two orthorhombic phases (O) with in-plane (O_{ip}) and out-of-plane (O_{op}) polarization directions, one rhombohedral (R) phase with deviated polarization directions (R_D), and a "Mix" region with multiple phases coexisting. In comparison to the monodomain temperature-misfit strain phase diagram[28] of KNN calculated from the thermodynamic model,[37] the temperature-misfit strain phase diagram established in this work considers the presence of multiple domains and phases and thus exhibits richer phase regions and boundaries.

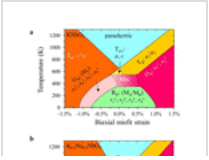

FIG. 1.

Temperature-misfit strain phase diagrams of (a) $KNbO_3$ and (b) $K_{0.5}Na_{0.5}NbO_3$ and (c) misfit strain-composition phase diagram at

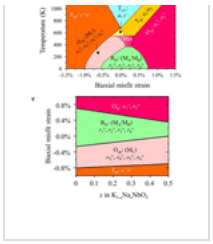

the room temperature of $K_{1-x}Na_xNbO_3$ ($0 \le x \le 0.5$) (001)-oriented thin films. The tetragonal, orthorhombic, and rhombohedral ferroelectric phases are denoted by T, O, and R, respectively. The subscripts "op" and "ip" stand for out-of-plane and in-plane, respectively, to denote the macroscopic polarization direction in each region. "D" stands for "Distorted." Mix represents the region with a mixture of domain structures of neighboring regions. Domain variants present in each region are given by italic lowercase letters, and the corresponding polarization directions are detailed in Fig. 2.

PPT | High-resolution

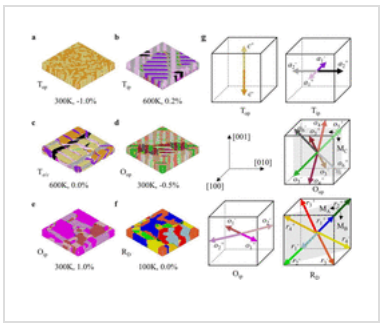

FIG. 2.

Representative domain structures of $K_{0.5}Na_{0.5}NbO_3$ thin films under various temperature and equibiaxial misfit strain conditions. The symbols for each phase are consistent with those in Fig. 1. The color code and polarization direction of each type of domain variant are given in (g). The shaded planes in O_{op} and R_D phases illustrate the polarization rotation planes for the presence of monoclinic phases (M_A, M_B, and M_C).

PPT | High-resolution

The phase diagrams of $KNbO_3$ and $K_{0.5}Na_{0.5}NbO_3$ are morphologically similar to each other except for the shifts of phase boundaries. For example, in both cases, the T-C transition temperature increases with both compressive and tensile strains, yet the T-C transition temperature of $K_{0.5}Na_{0.5}NbO_3$ is always higher than that of $KNbO_3$ under the same misfit strain, which is consistent with their stress-free bulk single crystal states.[27] Likewise, in the phase diagram of bulk KNN, the O phase has a broader temperature window in $K_{0.5}Na_{0.5}NbO_3$ than in $KNbO_3$, which can be identified in the thin-film phase diagrams, i.e., the O_{op} and O_{ip} regions are larger in $K_{0.5}Na_{0.5}NbO_3$ films. In this sense, the composition and misfit strain dependences of phase transition temperatures in KNN are relatively independent. It should be pointed out that both phase diagrams of KNN thin films resemble that of $BaTiO_3$ thin films obtained by phase-field simulations[38] because of the identical phase transition sequence (i.e., R-O-T-C upon heating) in their bulk states. However, the slopes of T-O and O-R transitions as a function of misfit strain change sharply at low temperatures, seen as the bent phase boundaries, which is in stark contrast to the straight lines seen in Fig. 2 of Ref. 38. This insensitivity of interferroelectric transitions to misfit strains close to 0 K is likely due to the

insensitivity of interferroelectric transitions to misfit strains close to 0 K is likely due to the non-negligible effect of quantum fluctuation,[39] which is incorporated in the LGD potential[27,28] of KNN but not in that of $BaTiO_3$ in Ref. 38. Besides, the misfit strain-composition phase diagram in Fig. 1(c) exhibits almost linear phase boundaries with small slopes with respect to the change of composition, perhaps due to the assumption of linear dependences in the Landau and electrostrictive coefficients on the sodium composition. Note that all phase boundaries in Fig. 1 can be of first-ordered-type and thus can have phase coexistence, which will be demonstrated in the following.

We now turn to analyze representative domain structures of each phase region, using the $K_{0.5}Na_{0.5}NbO_3$ thin film [Fig. 1(b)] as an example. The T_{op} phase is stable under large compressive strains. The corresponding domain structure is shown in Fig. 2(a), which has equal volume fractions of c_+ and c_- domain variants delineated by meandering 180° domain walls. The T_{ip} phase can be found in the upper-right region of the diagram adjacent to the paraelectric-ferroelectric transition. This region is represented by a_1/a_2 twinning domain structures [Fig. 2(b)] with a stripelike pattern along $\langle 110\rangle_{pc}$ separated by 90° domain walls. Therefore, compressive misfit strains favor domains with out-of-plane polarization (c_+/c_-), while tensile misfit strains favor domains with in-plane polarization (a_1/a_2), which agrees with previous results for other perovskite thin-film ferroelectrics.[14] In the middle of T_{op} and T_{ip} regions, one can find a $T_{a/c}$ region where a mixture of in-plane tetragonal domains are embedded within an out-of-plane tetragonal domain matrix, forming the ferroelastic a/c domain structure with slightly tilted 90° domain walls[36] [Fig. 2(c)]. This ferroelastic twinning structure has also often been observed in PZT thin films.[40,41]

At lower temperatures, the O_{op} phase tends to become stable in thin films under compressive strains, which is composed of eight domain variants with out-of-plane polarization ($o_3^{\pm} - o_6^{\pm}$). The domain morphology on the film surface is also stripelike with $\langle 110\rangle_{pc}$ domain walls [Fig. 2(d)], similar to that of a_1/a_2 domains in the T_{ip} phase. However, the out-of-plane polarization can be alternating, leading to finer features as observed in vertical PFM phase images.[12] Meanwhile, there exist four types of electrically neutral domain walls with 60°, 90°, 120°, and 180° rotation of polar vectors across them. With a tensile constraint, the O_{ip} phase become stable upon cooling, which consists of four domain variants ($o_1^{\pm} - o_2^{\pm}$) with an in-plane polarization. The corresponding domain structure is squarelike with 90° domain walls along $[\pm 100]_{pc}$ or $[0 \pm 10]_{pc}$ and 180° domain walls along $[\pm 1 \pm 10]_{pc}$ on the (001) film surface, as shown in Fig. 2(e). At further lower temperatures, $K_{0.5}Na_{0.5}NbO_3$ thin films subject to a moderate strain transform into the distorted rhombohedral phase R_D. Consequently, the typical domain structure has eight equivalent domain variants ($r_1^{\pm} - r_4^{\pm}$) separated by three types of domain walls (71°, 109°, and 180°), as shown in Fig. 2(f), similar to that of room-temperature rhombohedral $BiFeO_3$ thin films.[42,43]

Aside from single-phase regions described above, there are heterophase regions where

Aside from single-phase regions described above, there are heterophase regions where multiple phases coexist due to the first-order nature of these interferroelectric transitions. The heterophase domains can be found not only within the Mix phase region, which is near the tricritical points of multiple phases predicted by previous thermodynamic analysis,[28] but also near the boundaries of other single-phase regions. Several examples of heterophase domain structures are given in Fig. 3 along with the corresponding statistics on the volume fraction of each domain variant. Figure 3(a) shows the coexistence of R_D and O_{op} phases near their phase boundary. On the film surface, the latter exhibits $\langle 110\rangle_{pc}$-oriented stripes embedded within an R_D matrix. The coexistence of T_{op} and O_{op} phases in Fig. 3(b) has a different configuration where the c_+/c_- domains of the T_{op} phase "glue" a few patches of stripelike domains of O_{op}. The third example in Fig. 3(c) is within the Mix region, where the coexistence of three phases (O_{ip}, O_{op}, and R_D) can be observed. Domains of O_{ip} and O_{op} phases are interweaved, forming a distinctive domain pattern with $\langle 100\rangle_{pc}$ stripes that are absent in those single O-phase regions, while R_D domains are "squeezed" into the junctions of O_{ip} and O_{op} phases. An intriguing domain pattern with the coexistence of almost all domain variants is identified at 550 K under a zero misfit strain, as shown in Fig. 3(d). A checker-board pattern with quasitwo-dimensional periodicity is observed, which resembles the Piezoresponse Force Microscopy (PFM) images of a 52 nm $K_{0.9}Na_{0.1}NbO_3$ thin film on a $TbScO_3$ substrate.[21] The final example shows a coexistence of two in-plane phases at the phase boundary between T_{ip} and O_{ip} at high temperature. Similar to the configuration of Fig. 3(a), the stripelike domains of T_{ip} are embedded within a matrix of O_{ip} domains [Fig. 3(e)].

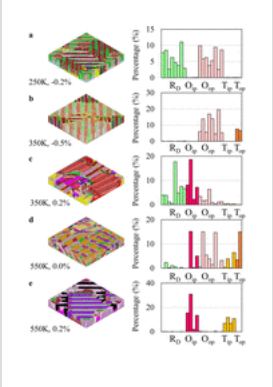

FIG. 3.

Histograms of volume fractions of each domain variant in five representative domain structures of $K_{0.5}Na_{0.5}NbO_3$ thin films under various temperature and misfit strain conditions where multiple phases coexist.

PPT | High-resolution

The phase coexistence has been recognized as a fingerprint for enhanced dielectric and piezoelectric properties due to the flattened free-energy landscapes and the associated ease of polarization rotation/extension.[44] In ferroelectric-based bulk crystals, phase coexistence can occur by tuning the chemical composition to approaching the morphotropic phase boundary or by engineering the interferroelectric phase transition temperatures, known as the thermotropic phase boundary.[45] In thin-film perovskite ferroelectrics, phase boundaries and phase coexistence can be created by tailoring the substrate constraints.[46] For example, in a chemically modified KNN thin film, Luo *et al.* showed the coexistence of low-symmetry

monoclinic phases at elevated temperatures and the associated enhanced piezoelectricity.[26] Therefore, we expect that the heterophase domain structures predicted in this work under various combinations of temperatures and misfit strains may as well exhibit enhanced dielectric and piezoelectric responses.

It is worth noting that different conventions have been adopted to represent the domain structures and phases in ferroelectric thin films.[38,47] For clarity, we have compared three different notation conventions that have been utilized to denote the phase regions in the temperature-misfit strain phase diagrams of perovskite ferroelectric thin films, along with the corresponding symbols and space groups of phases for bulk crystals, as shown in Table I. For instance, the nominal polarization in undistorted $o_3^{\pm} - o_6^{\pm}$ domains is along $[\pm 10 \pm 1]_{pc}$ or $[0 \pm 1 \pm 1]_{pc}$, but it can be deviated from the nominal directions due to the effect of misfit strains, thus inducing M_C-like phases [Fig. 2(g)]. Both the M_C phase and the stripelike domain morphology have been observed recently by PFM imaging in $K_{0.5}Na_{0.5}NbO_3$ thin films grown on $SrTiO_3$ substrates by sol-gel methods.[13,26] Likewise, the rhombohedral domain can be distorted into M_A and M_B like domains under compressive and tensile misfit strains, respectively, as also illustrated in Fig. 2(g).

TABLE I. Symbols of phases in temperature-misfit strain phase diagrams of perovskite ferroelectric thin films.

As a final example, we compare one of our simulated domain structures (20 nm $K_{0.5}Na_{0.5}NbO_3$ at 300 K under −0.5% misfit strain) with the PFM image obtained on a 35 nm $K_{0.7}Na_{0.3}NbO_3$ grown on a (011) $TbScO_3$ substrate in Fig. 4, as reported in Ref. 19 (equivalent to an anisotropic in-plane misfit strain of $\varepsilon_{11} = -0.6\%$ and $\varepsilon_{22} = -0.8\%$, recalculated from Ref. 12). One can find remarkable similarities between the experimental image and simulated results in terms of the stripelike pattern and the presence of four variants of domain bundles with mutually orthogonal in-plane polarizations (i.e., superdomains), even though the misfit strain states are not exactly the same. Moreover, the simulated domain structure resides in the O_{op} phase with polarization slightly slanted from $[\pm 10 \pm 1]_{pc}$ or $[0 \pm 1 \pm 1]_{pc}$ directions, which is consistent with the M_C phase reported in Ref. 19. Besides, a similar stripelike domain configuration has also been observed in $K_{0.5}Na_{0.5}NbO_3$ bulk polycrystals.[48] More detailed comparisons with the domain structures reported by Schmidbauer *et al.*[12,20,21] need to take into account the thickness effect, anisotropic misfit strain, and possibly strain relaxations, which will be explored in the future works. Very recently, Helden *et al.*[49] reported a huge impact of compressive strain on phase transition temperatures in epitaxial KNN thin films. Our theoretical predictions qualitative match the experimental results, albeit discrepancies in the chemical compositions, anisotropic constraints, and film thicknesses of

samples. A systematic and quantitative comparison will be exciting and is left for future works.

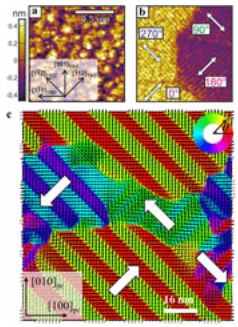

FIG. 4.

Experimental observation of the (a) surface morphology and (b) phase of lateral PFM images of a 35 nm $K_{0.7}Nb_{0.3}NbO_3$ film on a (110) $TbScO_3$ substrate. Adapted from L. von Helden, M. Schmidbauer, S. Liang, M. Hanke, R. Wördenweber, and J. Schwarzkopf, Nanotechnology 29, 415704 (2018). Copyright 2018 Institute of Physics. (b) Simulated domain pattern and polarization configuration on the top surface of a $K_{0.5}Na_{0.5}NbO_3$ thin film at 300 K under −0.5% biaxial misfit strain by phase-field simulations. The colors indicate the angle θ between the in-plane polarization vectors with the $[100]_{pc}$ direction.

PPT | High-resolution

In summary, we have established the temperature-strain phase diagrams of (001)-oriented $KNbO_3$ and $K_{0.5}Na_{0.5}NbO_3$ thin films and the misfit strain-composition phase diagram of $K_{1-x}Na_xNbO_3$ ($0 \le x \le 0.5$) thin films based on 3D polydomain structures generated using phase-field simulations. The temperature-strain phase diagrams of $KNbO_3$ and $K_{0.5}Na_{0.5}NbO_3$ are akin to each other with several single-phase and heterophase regions, which are morphologically similar to that of $BaTiO_3$ thin films. The representative domain structures are presented for each region and agree well with experimental observations. In particular, there are heterophase regions with the coexistence of multiple ferroelectric phases and complex domain structures, in which enhanced dielectric permittivity and piezoelectricity are anticipated. The present work provides theoretical guidance for exploring the strain engineering of KNN thin films with optimized functional properties.

B.W. and L.-Q.C appreciate the support from the National Science Foundation (NSF)-Materials Research Science and Engineering Center (MRSEC) under Grant Nos. DMR-1420620 and DMR-1744213. J.-J.W and L.-Q.C appreciate the support from the Army Research Office under Grant No. W911NF-17-1-0462. This work used the Extreme Science and Engineering Discovery Environment (XSEDE) Bridges at the Pittsburgh Supercomputing Center through allocation No. TG-DMR170006, which is supported by the National Science Foundation under Grant No. ACI-154856252. The authors appreciate Dr. von Helden and Dr. Jutta Schwarzkopf at the Leibniz Institute for Crystal Growth for insightful discussions and comments on the original manuscript.

REFERENCES

1. J. Rödel and J.-F. Li, MRS Bull. **43**, 576 (2018). https://doi.org/10.1557/mrs.2018.181, **Google Scholar**, **Crossref**

2. J. F. Li, K. Wang, F. Y. Zhu, L. Q. Cheng, and F. Z. Yao, J. Am. Ceram. Soc. **96**, 3677 (2013). https://doi.org/10.1111/jace.12715, **Google Scholar**, **Crossref**

3. J.-F. Li, K. Wang, B.-P. Zhang, and L.-M. Zhang, J. Am. Ceram. Soc. **89**, 706 (2006). https://doi.org/10.1111/j.1551-2916.2005.00743.x, **Google Scholar**, **Crossref**

4. K. Wang, B. Malič, and J. Wu, MRS Bull. **43**, 607 (2018). https://doi.org/10.1557/mrs.2018.178, **Google Scholar**, **Crossref**

5. J. Wu, D. Xiao, and J. Zhu, Chem. Rev. **115**, 2559 (2015). https://doi.org/10.1021/cr5006809, **Google Scholar**, **Crossref**

6. F. Yao, K. Wang, L. Cheng, X. Zhang, W. Zhang, F. Zhu, and J. Li, J. Am. Ceram. Soc. **98**, 448 (2015). https://doi.org/10.1111/jace.13265, **Google Scholar**, **Crossref**

7. P. Li, J. Zhai, B. Shen, S. Zhang, X. Li, F. Zhu, and X. Zhang, Adv. Mater. **30**, 1705171 (2018). https://doi.org/10.1002/adma.201705171, **Google Scholar**, **Crossref**

8. Y. Saito, H. Takao, T. Tani, T. Nonoyama, K. Takatori, T. Homma, T. Nagaya, and M. Nakamura, Nature **432**, 84 (2004). https://doi.org/10.1038/nature03028, **Google Scholar**, **Crossref**

9. S. Trolier-Mckinstry and P. Muralt, J. Electroceramics **12**, 7

(2004). https://doi.org/10.1023/B:JECR.0000033998.72845.51, **Google Scholar**, **Crossref**

10. T. Saito, T. Wada, H. Adachi, and I. Kanno, Jpn. J. Appl. Phys., Part 1 **43**, 6627 (2004). https://doi.org/10.1143/JJAP.43.6627, **Google Scholar**, **Crossref**

11. K. Tanaka, K. Kakimoto, and H. Ohsato, J. Cryst. Growth **294**, 209 (2006). https://doi.org/10.1016/j.jcrysgro.2006.05.041, **Google Scholar**, **Crossref**

12. J. Schwarzkopf, D. Braun, M. Hanke, R. Uecker, and M. Schmidbauer, Front. Mater. **4**, 26 (2017). https://doi.org/10.3389/fmats.2017.00026, **Google Scholar**, **Crossref**

13. J. Luo, W. Sun, Z. Zhou, H. Y. Lee, K. Wang, F. Zhu, Y. Bai, Z. J. Wang, and J. F. Li, Adv. Electron. Mater. **3**, 1700226 (2017). https://doi.org/10.1002/aelm.201700226, **Google Scholar**, **Crossref**

14. D. G. Schlom, L.-Q. Chen, C.-B. Eom, K. M. Rabe, S. K. Streiffer, and J.-M. Triscone, Annu. Rev. Mater. Res. **37**, 589 (2007). https://doi.org/10.1146/annurev.matsci.37.061206.113016, **Google Scholar**, **Crossref**

15. C. Paillard, S. Prokhorenko, and L. Bellaiche, Npj Comput. Mater. **5**, 6 (2019). https://doi.org/10.1038/s41524-018-0141-4, **Google Scholar**, **Crossref**

16. J. J. Wang, Y. Wang, J. F. Ihlefeld, P. E. Hopkins, and L. Q. Chen, Acta Mater. **111**, 220 (2016). https://doi.org/10.1016/j.actamat.2016.03.069, **Google Scholar**, **Crossref**

17. S. Pandya, G. A. Velarde, R. Gao, A. S. Everhardt, J. D. Wilbur, R. Xu, J. T. Maher, J. C. Agar, C. Dames, and L. W. Martin, Adv. Mater.

31, 1803312 (2019). https://doi.org/10.1002/adma.201803312, **Google Scholar**, **Crossref**

18. J. Hwang, Z. Feng, N. Charles, X. R. Wang, D. Lee, K. A. Stoerzinger, S. Muy, R. R. Rao, D. Lee, R. Jacobs, D. Morgan, and Y. Shao-horn, " Tuning perovskite oxides by strain: Electronic structure, properties, and functions in (electro)catalysis and ferroelectricity," Mater. Today (in press). https://doi.org/10.1016/j.mattod.2019.03.014, **Google Scholar**, **Crossref**

19. L. von Helden, M. Schmidbauer, S. Liang, M. Hanke, R. Wördenweber, and J. Schwarzkopf, Nanotechnology **29**, 415704 (2018). https://doi.org/10.1088/1361-6528/aad485, **Google Scholar**, **Crossref**

20. D. Braun, M. Schmidbauer, M. Hanke, A. Kwasniewski, and J. Schwarzkopf, Appl. Phys. Lett. **110**, 232903 (2017). https://doi.org/10.1063/1.4985191, **Google Scholar**, **Scitation**, **ISI**

21. D. Braun, M. Schmidbauer, M. Hanke, and J. Schwarzkopf, Nanotechnology **29**, 015701 (2018). https://doi.org/10.1088/1361-6528/aa98a4, **Google Scholar**, **Crossref**

22. M. Schmidbauer, M. Hanke, A. Kwasniewski, D. Braun, L. von Helden, C. Feldt, S. J. Leake, and J. Schwarzkopf, J. Appl. Crystallogr. **50**, 519 (2017). https://doi.org/10.1107/S1600576717000905, **Google Scholar**, **Crossref**

23. J. Schwarzkopf, D. Braun, M. Hanke, A. Kwasniewski, J. Sellmann, and M. Schmidbauer, J. Appl. Crystallogr. **49**, 375 (2016). https://doi.org/10.1107/S1600576716000182, **Google Scholar**, **Crossref**

24. I. Fujii and T. Wada, Jpn. J. Appl. Phys., Part 1 **55**, 10TA02 (2016). https://doi.org/10.7567/JJAP.55.10TA02, **Google Scholar**, **Crossref**

25. M. Schmidbauer, D. Braun, T. Markurt, M. Hanke, and J. Schwarzkopf, Nanotechnology **28**, 24LT02 (2017). https://doi.org/10.1088/1361-6528/aa715a, **Google Scholar**, **Crossref**

26. J. Luo, W. Sun, Z. Zhou, Y. Bai, Z. J. Wang, G. Tian, D. Chen, X. Gao, F. Zhu, and J.-F. Li, ACS Appl. Mater. Interfaces **9**, 13315 (2017). https://doi.org/10.1021/acsami.7b02263, **Google Scholar**, **Crossref**

27. H. Pohlmann, J. J. Wang, B. Wang, and L. Q. Chen, Appl. Phys. Lett. **110**, 102906 (2017). https://doi.org/10.1063/1.4978360, **Google Scholar**, **Scitation**, **ISI**

28. M. J. Zhou, J. J. Wang, L. Q. Chen, and C. W. Nan, J. Appl. Phys. **123**, 154106 (2018). https://doi.org/10.1063/1.5027505, **Google Scholar**, **Scitation**, **ISI**

29. L.-Q. Chen, J. Am. Ceram. Soc. **91**, 1835 (2008). https://doi.org/10.1111/j.1551-2916.2008.02413.x, **Google Scholar**, **Crossref**

30. J.-J. Wang, B. Wang, and L.-Q. Chen, Annu. Rev. Mater. Res. **49**, 127 (2019). https://doi.org/10.1146/annurev-matsci-070218-121843, **Google Scholar**, **Crossref**

31. I. Tomeno, Y. Tsunoda, K. Oka, M. Matsuura, and M. Nishi, Phys. Rev. B **80**, 104101 (2009). https://doi.org/10.1103/PhysRevB.80.104101, **Google Scholar**, **Crossref**

32. L. E. Cross and G. A. Rossetti, J. Appl. Phys. **69**, 896 (1991).

https://doi.org/10.1063/1.3473330, **Google Scholar**, **Scitation**, **ISI**

33. H. Uršič, A. Benčan, M. Škarabot, M. Godec, and M. Kosec, J. Appl. Phys. **107**, 033705 (2010). https://doi.org/10.1063/1.3291119, **Google Scholar**, **Scitation**, **ISI**

34. N. Ishizawa, J. Wang, T. Sakakura, Y. Inagaki, and K. I. Kakimoto, J. Solid State Chem. **183**, 2731 (2010). https://doi.org/10.1016/j.jssc.2010.09.018, **Google Scholar**, **Crossref**

35. L. Q. Chen and J. Shen, Comput. Phys. Commun. **108**, 147 (1998). https://doi.org/10.1016/S0010-4655(97)00115-X, **Google Scholar**, **Crossref**

36. Y. L. Li, S. Y. Hu, Z. K. Liu, and L. Q. Chen, Acta Mater. **50**, 395 (2002). https://doi.org/10.1016/S1359-6454(01)00360-3, **Google Scholar**, **Crossref**

37. N. A. Pertsev, A. G. Zembilgotov, and A. K. Tagantsev, Phys. Rev. Lett. **80**, 1988 (1998). https://doi.org/10.1103/PhysRevLett.80.1988, **Google Scholar**, **Crossref**

38. Y. L. Li and L. Q. Chen, Appl. Phys. Lett. **88**, 072905 (2006). https://doi.org/10.1063/1.2172744, **Google Scholar**, **Scitation**, **ISI**

39. E. K. H. Salje, B. Wruck, and H. Thomas, Z. Phys. B Condens. Matter **82**, 399 (1991). https://doi.org/10.1007/BF01357186, **Google Scholar**, **Crossref**

40. M. Li, B. Wang, H.-J. Liu, Y.-L. Huang, J. Zhang, X. Ma, K. Liu, D. Yu, Y.-H. Chu, L.-Q. Chen, and P. Gao, Acta Mater. **171**, 184 (2019). https://doi.org/10.1016/j.actamat.2019.04.003, **Google Scholar**, **Crossref**

41. V. Nagarajan, A. Roytburd, A. Stanishevsky, S. Prasertchoung, T. Zhao, L. Chen, J. Melngailis, O. Auciello, and R. Ramesh, Nat. Mater. **2**, 43 (2003). https://doi.org/10.1038/nmat800, **Google Scholar**, **Crossref**

42. J. X. Zhang, Y. L. Li, S. Choudhury, L. Q. Chen, Y.-H. H. Chu, F. Zavaliche, M. P. Cruz, R. Ramesh, and Q. X. Jia, J. Appl. Phys. **103**, 094111 (2008). https://doi.org/10.1063/1.2927385, **Google Scholar**, **Scitation**, **ISI**

43. Y. H. Chu, Q. Zhan, L. W. Martin, M. P. Cruz, P. L. Yang, G. W. Pabst, F. Zavaliche, S. Y. Yang, J. X. Zhang, L. Q. Chen, D. G. Schlom, I. N. Lin, T. B. Wu, and R. Ramesh, Adv. Mater. **18**, 2307 (2006). https://doi.org/10.1002/adma.200601098, **Google Scholar**, **Crossref**

44. D. Damjanovic and G. A. Rossetti, MRS Bull. **43**, 588 (2018). https://doi.org/10.1557/mrs.2018.157, **Google Scholar**, **Crossref**

45. T. T. A. Lummen, Y. Gu, J. Wang, S. Lei, F. Xue, A. Kumar, A. T. Barnes, E. Barnes, S. Denev, A. Belianinov, M. Holt, A. N. Morozovska, S. V. Kalinin, L. Q. Chen, and V. Gopalan, Nat. Commun. **5**, 3172 (2014). https://doi.org/10.1038/ncomms4172, **Google Scholar**, **Crossref**

46. R. J. Zeches, M. D. Rossell, J. X. Zhang, A. J. Hatt, Q. He, C. H. Yang, A. Kumar, C. H. Wang, A. Melville, C. Adamo, G. Sheng, Y. H. Chu, J. F. Ihlefeld, R. Erni, C. Ederer, V. Gopalan, L. Q. Chen, D. G. Schldin, N. A. Spaldin, L. W. Martin, and R. Ramesh, Science **326**, 977 (2009). https://doi.org/10.1126/science.1177046, **Google Scholar**, **Crossref**

47. V. G. Koukhar, N. A. Pertsev, and R. Waser, Phys. Rev. B **64**, 214103 (2001). https://doi.org/10.1103/PhysRevB.64.214103, **Google Scholar**, **Crossref**

48. F. Rubio-Marcos, A. Del Campo, R. López-Juárez, J. J. Romero, and J. F. Fernández, J. Mater. Chem. **22**, 9714 (2012). https://doi.org/10.1039/c2jm30483j, **Google Scholar**, **Crossref**

49. L. von Helden, L. Bogula, P.-E. Janolin, M. Hanke, T. Breuer, M. Schmidbauer, S. Ganschow, and J. Schwarzkopf, Appl. Phys. Lett. **114**, 232905 (2019). https://doi.org/10.1063/1.5094405, **Google Scholar**, **Scitation**, **ISI**

Published under license by AIP Publishing.

Resources

AUTHOR

LIBRARIAN

ADVERTISER

General Information

ABOUT

CONTACT

HELP

PRIVACY POLICY

TERMS OF USE

FOLLOW AIP PUBLISHING:

Website © 2019 AIP Publishing LLC. Article copyright remains as specified within the article.